Observation of photoacoustic/photothermal effect with a liquid-core optical ring resonator

Huanjing Guo (郭焕菁), Long Jin (金 龙)*, Jun Ma (马 军), and Bai-Ou Guan (关柏鸥)

Guangdong Provincial Key Laboratory of Optical Fiber Sensing and Communications, Institute of Photonics Technology, Jinan University, Guangzhou 510632, China

**Corresponding author: iptjinlong@gmail.com*

Received January 18, 2017; accepted April 14, 2017; posted online May 9, 2017

Photothermal/photoacoustic (PT/PA) spectroscopy provides useful knowledge about optical absorption, as well as the thermal and acoustical properties of a liquid sample. For microfluidic biosensing and bioanalysis where an extremely small volume of liquid sample is encapsulated, simultaneous PT/PA detection remains a challenge. In this work, we present a new optofluidic device based on a liquid-core optical ring resonator (LCORR) for the investigation of PT and PA effects in fluid samples. A focused 532 nm pulsed light optically heats the absorptive fluid in a capillary to locally create a transient temperature rise, as well as acoustic waves. A 1550 nm CW laser light is quadrature-locked to detect the resonance spectrum shift of the LCORR and study thermal diffusion and acoustic wave propagation in the capillary. This modality provides an optofluidic investigative platform for biological/biochemical sensing and spectroscopy.

OCIS codes: 230.5750, 350.5340, 110.5125.

doi: 10.3788/COL201715.072301.

Photothermal/photoacoustic (PT/PA) spectroscopy measures the absorption of a medium in an indirect manner—by detecting absorption-induced temperature change or acoustic waves[1,2]. It can also provide useful knowledge about the thermal and acoustic properties of the target sample. PT/PA detection has presented advanced capabilities for trace gas detection or biosensing/bioanalysis of liquid samples. Recently, PT/PA detection has achieved the single-molecular level. However, a simultaneous PT/PA measurement is still a challenge in a microfluidic system in which a liquid sample with an extremely small volume is encapsulated. A microfluidic channel or chip is typically integrated with a conductor-based temperature sensor for thermal detection or alternatively embedded on microphones or surface-acoustic wave sensors for acoustic detection[3,4]. An optical microcavity can circulate light many rounds and enable a strong optical resonance[5,6]. It is capable of measuring extremely weak perturbations and has been applied for biosensing[7,8]. Specifically, a liquid-core optical ring resonator (LCORR) can detect and analyze a liquid sample in an extremely small volume[9,10]. In this scheme, a silica capillary simultaneously acts as the microfluidic channel and an optical resonator. Recently, a number of new sensing mechanisms based on optomechanics, plasmonic interaction, as well as self-hydrodyning microlasers, have been proposed with LCORRs to provide additive information on the optical, acoustic, and thermal properties of the liquid sample, showing its great flexibility[11–13]. In this Letter, we demonstrate the observation of the PT/PA effect by use of an LCORR. A 532 nm pulse laser is focused into the interior absorptive liquid. The absorption induces a localized, transient temperature change, as well as pulsed acoustic waves. The PT effect induces a rapid heat-up process in the cavity wall, followed by a slow thermal decay. The PA effect causes local vibration of the capillary, and two counter-propagating acoustic waves can be excited. A train of ring-down PA signals can be observed as a result of the resonance nature of the tapered capillary. The thermally and acoustically induced resonance shifts are detected by reading out the transmission intensity of a quadrature-locked probe light. The LCORR offers a PT/PA investigative platform, which offers an alternative modality for biomedical sensing and spectroscopy in a microfluidic system.

Figure 1(a) shows a sketch of the LCORR for optical detection of the PT/PA effect. The silica capillary acts as a microfluidic channel as well as an optical ring resonator. A probe light is evanescently coupled to the resonator via a fiber taper. Optical resonance can be established with a $2m\pi$ round-trip optical path, where m is an integer. As a result, the transmission spectrum of the fiber taper presents multiple, periodic resonant dips. Each dip has an approximate Airy-function spectral profile. The capillary encapsulates an absorptive medium. A visible pulsed laser side-illuminates the interior fluid sample. The absorption of the laser pulses creates a localized temperature change via the PT effect. In the following moment, thermal diffusion can heat up the capillary and induce an optical phase change. The highly localized, transient thermal effect subsequently exerts a pressure wave via the PA effect. The pulsed pressure wave in the liquid medium can excite a local stress over the capillary, which induces an addictive optical phase modulation. Figure 1(b) schematically demonstrates how the PA/PT-induced optical response is measured. The phase modulation of the intracavity light by the thermal and acoustic waves causes a wavelength shift of the transmission spectrum. A quadrature-locked

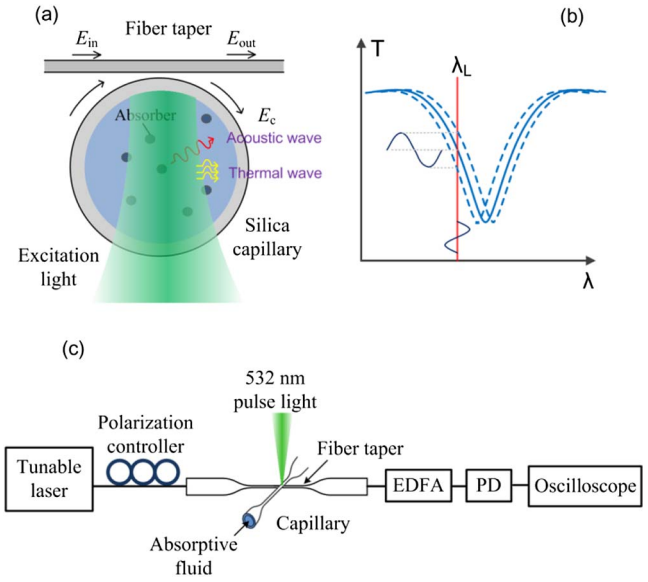

Fig. 1. (a) Schematic of the LCORR for PT/PA-effect observation. (b) Resonance-shift measurement. The transmission intensity of the quadrature-locked probe light is modulated by the PT/PA-induced resonance shift. (c) Experimental setup for optical detection of the PT/PA effect in an LCORR. PD, photodetector; EDFA, erbium-doped fiber amplifier.

probe laser, whose line width is much narrower than the spectral width of a resonance dip, is evanescently coupled into the cavity. It is difficult to measure the transmission spectrum at a rate of hundreds of megahertzs to detect the fast-varying acoustic signals. Therefore, this spectral change is translated to the variation in transmission intensity of the probe light in this work. Figure 1(c) shows the experimental setup. The silica capillary has outer and inner diameters of 850 and 700 μm, respectively. Its polymer jacket is removed before fusion tapering with a longitudinally scanning flame. The taper waist has a length of about 10 mm, an outer diameter of about 32 μm, and a thickness of 2.8 μm. The tapering process is carried out under atmospheric conditions, and the transverse shape is almost unchanged. The capillary is tapered down to a much smaller dimension to achieve a stronger thermal/acoustic response. The tapering process also greatly reduces the surface roughness and benefits the formation of a high-Q resonator. A black ink, as an absorptive fluid, is injected into the capillary with a microfluidic pump with a controllable flow rate. A linearly polarized 1550 nm tunable distributed feedback (DFB) semiconductor laser is used as a probe light. This laser is selected because its output wavelength can be tuned to overcome the random wavelength drift of the optical resonator, which is induced by environmental noise. Its output power is about 1 mW. The probe light is launched on the resonator via evanescent coupling with a micron-scaled fiber tapered from an ordinary single-mode optical fiber. The fiber taper has a waist diameter of about 3 μm. The fiber taper is orthogonally aligned with the capillary resonator to excite the whispering-gallery modes (WGMs). The gap distance between the fiber taper and the capillary is adjusted with two 3D linear stages to maximize the coupling ratio. This optimization is critical to achieve a sharp slope in the transmission spectrum. The output wavelength of the probe light is finely adjusted to the quadrature of the transmission dip, to maximize the optical response. A polarization controller is used to selectively excite the TE or TM mode in the resonator. A high-speed In/Ga/As photodetector (Thorlabs, DET08CFC/M) is used to record the variation in the transmission intensity. An oscilloscope with a sampling rate of 1 GHz monitors the optical response. An erbium-doped fiber amplifier is used to amplify the optical signal for a higher signal-to-noise ratio. Special care is taken to minimize thermal fluctuation and polarization variation, as well as vibrations of the devices, in order to obtain a stable output waveform.

Figure 2 shows a transmission spectrum of the LCORR, measured with an unpolarized broadband light source and an optical spectrum analyzer (OSA, Yokogawa, AQ6370C). The resonance wavelength of the LCORR is given by

$$\lambda = \frac{\pi D n_{\text{eff}}}{m}, \tag{1}$$

where D denotes the outer diameter of the capillary, n_{eff} represents the effective index of the optical mode that circulates in the resonator, and m is an integer. The resonant dips with the highest depths are a result of resonances of the fundamental radial modes. The multiple dips on the short wavelength side might be a result of WGMs with higher radial orders. The optical modes have very close effective indices, and the transmission dips have small wavelength separations. Higher-order mode resonances have lower dip depths as a result of weaker evanescent coupling strengths. The free-spectral range (FSR) is about 18.8 nm. A selected dip is enlarged and shown in Fig. 2, as

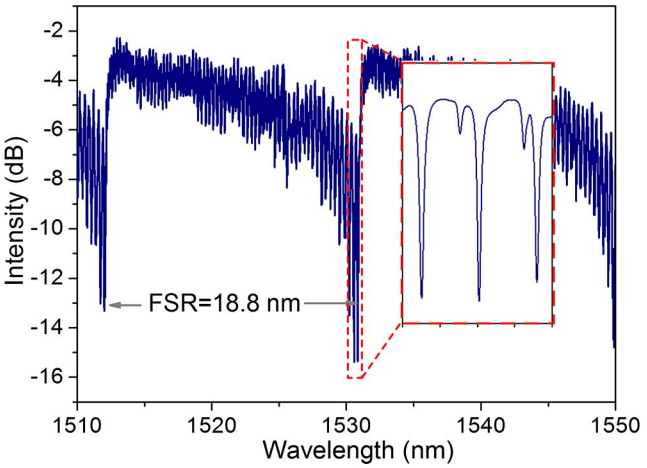

Fig. 2. Transmission spectrum of the resonator over a 50 nm wavelength range. Inset: enlarged spectrum near 1530 nm.

measured with a high-resolution (10 MHz) OSA. The dips have an average spectral width of 3.2 pm, corresponding to a Q factor of $\sim 4.8 \times 10^5$. When the resonator is subjected to a thermal or acoustic perturbation, Γ, the induced wavelength shift can be expressed by

$$\frac{\mathrm{d}\lambda}{\mathrm{d}\Gamma} = \lambda \cdot \left(\frac{1}{n_{\mathrm{eff}}} \frac{\mathrm{d}n_{\mathrm{eff}}}{\mathrm{d}\Gamma} + \frac{1}{D} \frac{\mathrm{d}D}{\mathrm{d}\Gamma} \right). \tag{2}$$

The wavelength shift can be translated to the variation in transmission intensity of the probe light, which follows a simple relation $\mathrm{d}I = \mathrm{d}\lambda \cdot S$, where S denotes the slope of the transmission dip at the quadrature. With the above equations, one can calculate the thermal/acoustic response of the resonator.

We then carry out PA/PT detection with the LCORR using the experimental configuration shown in Fig. 1. The repetition rate of the excitation light is 1 kHz. The single-pulse energy is 1 μJ. Figure 3 shows the superimposed PA and PT waveforms induced by a single laser pulse, measured with the LCORR. The laser pulse launched at the moment $t = 100$ μs. The absorption of a single laser pulse in the liquid sample creates a localized temperature rise. The heat diffuses into the capillary wall to heat up the intracavity light and induce a resonance change. The heat-up process takes about 10 μs. Then, the heat dissipates, mainly along the direction of the capillary length. As a result, the temperature slowly decreases, with a $1/e$ decay time of about 350 μs. The heat diffusion follows the heat transfer equation

$$\rho C_p \frac{\partial T(r,t)}{\partial t} = \nabla \cdot [\kappa \nabla T(r,t)] + Q(r,t), \tag{3}$$

where ρ, C_p, κ, and Q denote density, heat capacity, thermal conductivity, and volume heat source. The time-varying temperature distribution can be calculated with the provided initial temperature profile and boundary conditions by solving Eq. (3). In this case, the heat source term $Q(r,t)$ is ignored since the heat-up duration of the fluid, i.e., the time to transition from optical absorption to heat, is extremely short (ns scale). Figure 4(a) shows an axial symmetrical model for the calculation of the thermally induced response of the LCORR. The red zone represents the region heated by optical absorption, which is surrounded by the capillary, as well as the fluid, at room temperature. In this thermal diffusion model, the initial temperature of the hot zone is $Ts = T_0 + \Delta T$, where $T_0 = 273$ K and $\Delta T = 100$ K are the environmental temperature and the temperature rise, respectively.

The cylindrical "hot zone" has a radius of 13.2 μm and a height of 6 μm. The temperature is uniform over the cylinder for simplicity. Actually, the side illumination creates a nonuniform initial temperature profile over the cross section. However, considering that the induced optical phase is an integration effect and the temporal temperature variation of the silica wall is mainly determined by the temperature difference at the fluid–silica interface, the simplified model is reasonable. A continuous heat flux is assumed at the silica–liquid boundary. We set a boundary condition of thermal insulation at the outer surface of the capillary, considering the heat flux at the silica-air interface is relatively weak. In the calculation, the density, heat capacity, and thermal conductivity are 994 kg/m^3,

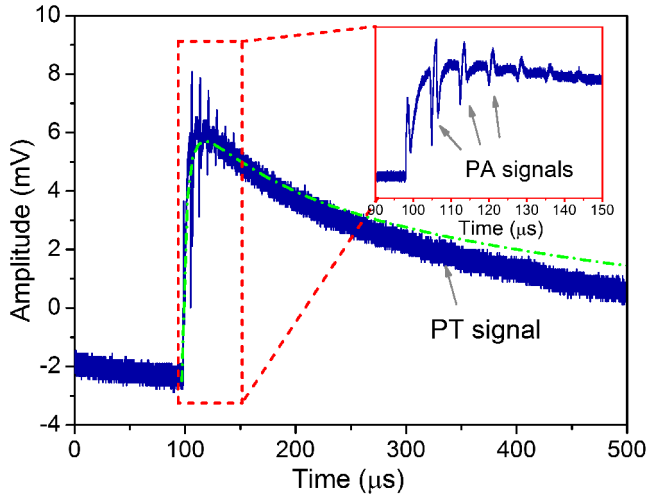

Fig. 3. (Color online) Measured waveform of PA and PT signals detected by the LCORR. The green dash-dot curve plots the calculated thermal response based on the model depicted in Fig. 4(a). Inset: close-up of the PA signals.

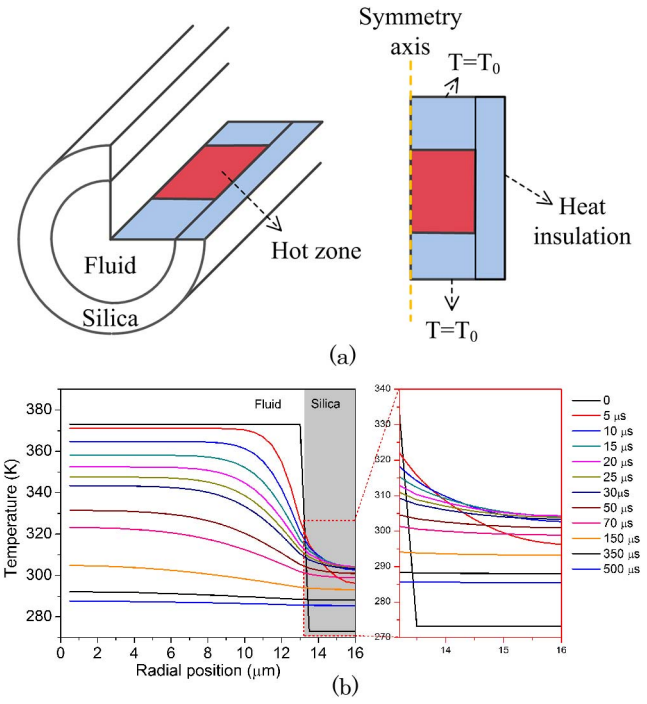

Fig. 4. (Color online) (a) Axial symmetrical model for the calculation of the thermally induced response of the LCORR. (b) Calculated evolution of radial temperature profile. Inset: enlarged result over the silica wall.

4200 J/(kg · K), and 0.626 W/(m · K) in the fluid domain and 2203 kg/m^3, 703 J/(kg · K), and 1.38 W/(m · K) in the solid domain. With this model and the boundary conditions, the temporal temperature distribution is numerically calculated by solving Eq. (3). Figure 4(b) shows the evolution of the radial temperature profile. It shows that the transient temperature rise is followed by a slow decay over the silica wall. The thermally induced intensity variation of the probe light can be further obtained by averaging the temperature change over the silica wall. In Fig. 3, we superimpose the calculated optical response as the dash-dot curve. For comparison, the amplitude of this curve is adjusted to be close to the measured result. Note that the amplitude of the signal is in proportion to the thermal expansion and thermo-optic coefficient of silica, the temperature difference, ΔT, and the slope of the transmission dip, S. However, the temperature rising and decaying times are not relevant with these parameters, and this treatment is reasonable. The slight deviation of the calculated curves may be a result of the inaccuracy of the employed thermal expansion coefficients. The PT signals are weakened with higher repetition rates since the pulse interval is not sufficient for the device to fully recover to the original temperature. For repetition rates over 15 kHz, the PT signals can hardly be observed. In this case, the excitation light can be approximately treated as a continuous heat source, and a thermal-equilibrium model is more suitable to describe this problem.

Figure 3 also exhibits a series of fast-varying PA signals that are superimposed on the PT waveform. We have extracted the PA signals and replotted them in Fig. 5(a) for better visualization. We used a bandpass filter in signal processing to suppress the noise level. The absorption of a nanosecond-duration laser pulse also creates a highly localized pressure change. The pressure wave propagates as a spherical ultrasound pulse. The acoustic signal can be coupled to the silica capillary and induce its in-plane vibration. The local vibration corresponds to the first waveform in the series in Fig. 5(a). Note that the tapered capillary can also act as an acoustic waveguide as a result of its line shape. This vibration also excites propagating acoustic waves toward the forward and backward directions along the capillary length. The velocity and mode profiles of the propagating modes can be obtained by solving wave equations over the fluid and the solid domains. The interaction between the silica capillary and the interior fluid is engaged by local pressure in the fluid that exerts force on the shell and by the normal acceleration of the capillary wall. As a result, the acoustic eigenmodes, which describe the displacement field in the solid domain and the pressure wave field in the fluid domain, can be determined. The LCORR can only detect circularly symmetrical modes because higher-order azimuthal modes have a self-compensation effect in the optical phase over a round-trip. These waves are reflected at the boundaries between the uniform taper waist and the transition regions as a result of the abrupt geometrical nonuniformity. After a round-trip propagation, the two pulses reunite at the excitation location and create the second pulse waveform in Fig. 5(a). This process is repeated several times, yielding periodic waveforms until the acoustic waves almost decay. Considering the 10 mm waist length of the capillary, the 7.5 μs period corresponds to a propagation velocity of 2666 m/s for the propagating acoustic wave. Figure 5(a) inset shows an enlarged single PA waveform, which reflects the frequency profile of the excited PA signals.

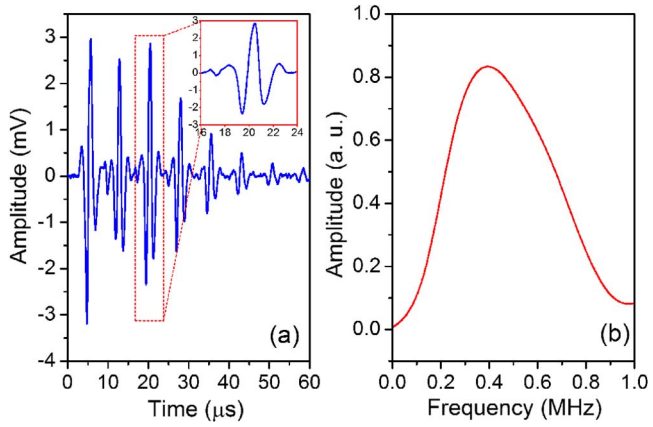

Fig. 5. (a) PA waveform series extracted from Fig. 3. Inset: enlarged single PA waveform. (b) Frequency response.

In conclusion, we present a new optofluidic platform based on an LCORR for the investigation of PT and PA effects in a fluid sample. The PT and PA effects are simultaneously excited with a nanosecond-pulse laser. The induced thermal effect and pressure waves are detected by monitoring the transmission of a quadrature-locked probe laser. This modality provides an alternative approach for biological/biochemical sensing and spectroscopy in microfluidics. It can provide additive information for the encapsulated microfluid, including optical absorption as well as thermal and acoustic properties.

This work was supported by the National Natural Science Foundation of China (No. 11374129) and the Planned Science & Technology Project of Guangzhou (No. 2014J2200003).

References

1. S. E. Bialkowski, *Photothermal Spectroscopy Methods for Chemical Analysis* (Wiley, 1996).
2. A. A. Kosterev, Y. A. Bakhirkin, R. F. Curl, and F. K. Tittel, Opt. Lett. **27**, 1902 (2002).
3. S. E. Johnston, K. E. Fadgen, and J. W. Jorgenson, Anal. Chem. **78**, 5309 (2006).
4. R. Kishor, F. Gao, S. Sreejith, X. Feng, Y. P. Seah, Z. Wang, M. C. Stuparu, T.-T. Lim, X. Chen, and Y. Zheng, RSC Adv. **6**, 50238 (2016).
5. J. Huang, J. Yang, H. Zhang, H. Wang, W. Wu, D. Chen, and S. Chang, Chin. Opt. Lett. **14**, 101301 (2016).
6. J. Cheng and N. Yan, Chin. Opt. Lett. **13**, 082201 (2015).
7. X. Fan and I. M. White, Nat. Photon. **5**, 591 (2011).

8. A. L. Washburn, L. C. Gunn, and R. C. Bailey, Anal. Chem. **81**, 9499 (2009).
9. I. M. White, H. Oveys, and X. Fan, Opt. Lett. **31**, 1319 (2006).
10. M. Li, X. Wu, L. Liu, X. Fan, and L. Xu, Anal. Chem. **85**, 9328 (2013).
11. K. Han, J. H. Kim, and G. Bahl, Optica **3**, 585 (2016).
12. M. D. Baaske, M. R. Foreman, and F. Vollmer, Nat. Nanotechnol. **9**, 933 (2014).
13. L. He, S. K. Özdemir, J. Zhu, W. Kim, and L. Yang, Nat. Nanotechnol. **6**, 428 (2011).